Mouse Emi2 as a distinctive regulatory hub in second meiotic metaphase

Toru Suzuki[1,2], Emi Suzuki[2], Naoko Yoshida[2], Atsuko Kubo[2], Hongmei Li[2], Erina Okuda[2], Manami Amanai[2] and Anthony C. F. Perry[1,2,*]

SUMMARY

The oocytes of vertebrates are typically arrested at metaphase II (mII) by the cytostatic factor Emi2 until fertilization. Regulatory mechanisms in *Xenopus* Emi2 (xEmi2) are understood in detail but contrastingly little is known about the corresponding mechanisms in mammals. Here, we analyze Emi2 and its regulatory neighbours at the molecular level in intact mouse oocytes. Emi2, but not xEmi2, exhibited nuclear targeting. Unlike xEmi2, separable N- and C-terminal domains of mouse Emi2 modulated metaphase establishment and maintenance, respectively, through indirect and direct mechanisms. The C-terminal activity was mapped to the potential phosphorylation target Tx_5SxS, a destruction box (D-box), a lattice of Zn^{2+}-coordinating residues and an RL domain. The minimal region of Emi2 required for its cytostatic activity was mapped to a region containing these motifs, from residue 491 to the C terminus. The cytostatic factor Mos-MAPK promoted Emi2-dependent metaphase establishment, but Mos autonomously disappeared from meiotically competent mII oocytes. The N-terminal Plx1-interacting phosphodegron of xEmi2 was apparently shifted to within a minimal fragment (residues 51-300) of mouse Emi2 that also contained a calmodulin kinase II (CaMKII) phosphorylation motif and which was efficiently degraded during mII exit. Two equimolar CaMKII γ isoform variants were present in mII oocytes, neither of which phosphorylated Emi2 in vitro, consistent with the involvement of additional factors. No evidence was found that calcineurin is required for mouse mII exit. These data support a model in which mammalian meiotic establishment, maintenance and exit converge upon a modular Emi2 hub via evolutionarily conserved and divergent mechanisms.

KEY WORDS: Emi2, Metaphase II, Mammalian meiosis, *Xenopus*

INTRODUCTION

The meiotic cell cycle of fertilizable oocytes in vertebrates is typically restrained at the second metaphase (mII) by a cytostatic factor (CSF) to prevent development without a paternal genome (parthenogenesis). The underlying mechanisms of mII arrest and exit are best understood in *Xenopus* and relatively poorly in mammals. In both, mII arrest correlates with the kinase activity of maturation promoting factor (MPF), a heterodimer of Cyclin B (CycB) and the cyclin-dependent kinase Cdc2 (Masui and Markert, 1971; Gautier et al., 1989; Gautier et al., 1990; Perry and Verlhac, 2008). MPF is active in both mitotic and meiotic cell cycles in vertebrates, but its prolonged stabilization by CSF is unique to mII and results in mII arrest.

Exit from mII occurs when CycB undergoes destruction box- (D-box-) dependent ubiquitylation by the anaphase-promoting complex, APC, an E3 ubiquitin ligase; this targets CycB for 26S proteasomal hydrolysis and eliminates MPF, thereby inducing metaphase exit (Glotzer et al., 1991; Peters, 2006). Arrest at mII is achieved by suspending APC activity, which is the function of CSF. One CSF responsible for this inhibition is the endogenous meiotic inhibitor 2, Emi2, the activity of which is essential for mII arrest as independently revealed in *Xenopus* (Schmidt et al., 2005) and the mouse (Shoji et al., 2006). Depletion of Emi2 from intact

mouse oocytes causes mII release in a manner that requires the APC activator, Cdc20; one explanation of this is that Emi2 prevents Cdc20 from activating the APC (Shoji et al., 2006; Amanai et al., 2006).

Xenopus Emi2 (xEmi2) is stabilized during mII by phosphorylation from xMos to xMek to xMAPK to xRsk to xEmi2 (Sagata et al., 1989; Bhatt and Ferrell, 1999; Gross et al., 2000; Inoue et al., 2007; Nishiyama et al., 2007a) (Fig. 1). xRsk phosphorylates xEmi2 at S335, T336, S342 and S344. Phosphorylation at S335 and T336 facilitates the binding of protein phosphatase 2A (xPP2A), which in turn dephosphorylates phospho-residues at T545 and T551, and S213, T239, T252 and T267 (Wu et al., 2007b). Dephosphorylation of T545/T551 enhances binding of the xEmi2 C-terminal domain to the APC core component, xCdc27 (xAPC3) to inhibit the APC (Wu et al., 2007b) whereas dephosphorylation of the S213-T267 cluster stabilizes xEmi2 (Wu et al., 2007a). In *Xenopus*, xPP2A activity towards xEmi2 is thus stimulated by xMos via xRsk to promote mII arrest (Fig. 1).

In the mouse, *Mos null* oocytes fail to activate the MAPK pathway but nevertheless often arrest or pause at mII with MPF activity initially unaffected, or progress through mII and then 'collapse' back to mIII (Verlhac et al., 1996; Choi et al., 1996). Oocytes from *Mos*-null mice contain anomalously long, interphase-like microtubules during mI to mII and mII to mIII transitions (Verlhac et al., 1996). Emi2-depleted oocytes undergo aberrant cytokinesis (Shoji et al., 2006), but the relationship between Mos and Emi2 in the mammalian meiotic cell cycle remains unknown and meiotic coordination with spindle dynamics poorly understood.

Fertilization triggers an increase in the oocyte concentration of intracellular 'free' calcium, $[Ca^{2+}]_i$ (reviewed by Runft et al., 2002). In *Xenopus* oocyte extracts, this activates the Ca^{2+}-dependent

[1]Laboratory of Mammalian Molecular Embryology, Bath Centre for Regenerative Medicine, and Development of Biology and Biochemistry, University of Bath, Bath BA2 7AY, UK. [2]RIKEN Center for Developmental Biology, 2-2-3 Minatojima Minamimachi, Chuo-ku, Kobe 650-0047 Japan.

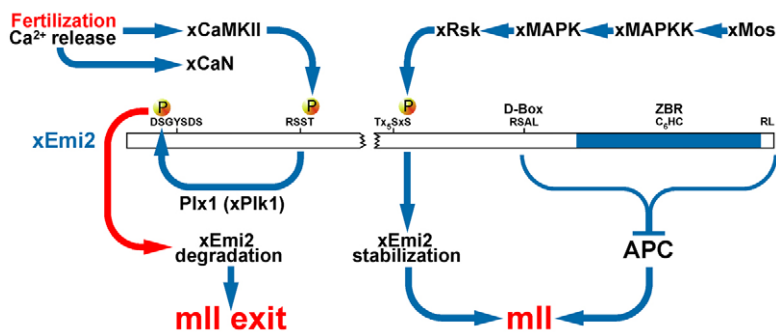*Author for correspondence (perry135@aol.com)

Fig. 1. *Xenopus* xEmi2 as meiotic regulatory hub. Diagram showing interactions between principal components of *Xenopus* meiotic homeostasis and xEmi2. APC, anaphase-promoting complex; xCaMKII, calmodulin kinase II; xCaN, calcineurin; D-box, destruction box; xEmi2, endogenous meiotic inhibitor 2; xMAPK, mitogen-activated protein (xMAP) kinase (xErk); xMAPKK, xMAP kinase kinase (xMek); xMos, Moloney sarcoma oncogene; Plx1, polo-like kinase 1; xRsk, ribosomal s6 kinase 1; ZBR, zinc-binding region.

enzymes calmodulin kinase II (CaMKII) and calcineurin (CaN) (Fig. 1). It is unclear whether xCaN regulates the APC directly through xEmi2, with support both for (Nishiyama et al., 2007b) and against (Mochida and Hunt, 2007). Activated xCaMKII phosphorylates xEmi2 at threonine 195 (T195) of its canonical motif, RXST (Rauh et al., 2005). xEmi2 phosphorylated at T195 is a favoured substrate for polo-like kinase, Plx1 (the counterpart of mammalian Plk1), which then phosphorylates xEmi2 at S33/S38 in the phosphodegron motif $DSGX_3S$, targeting xEmi2 for xβTrcp- (Trcpb-) dependent proteasomal destruction (Schmidt et al., 2005; Rauh et al., 2005).

These details await analysis in mammalian Emi2 but it already seems clear that mouse and *Xenopus* (x)Emi2 differ. The N-terminal Plx1 phosphodegron does not have an N-terminal mouse Emi2 counterpart (Rauh et al., 2005; Perry and Verlhac, 2008). Moreover, *Xenopus* xRsk links the Mos-MAPK cascade to xEmi2 but mouse oocytes lacking Rsk (those of *Rsk1*, *Rsk2*, *Rsk3* triple null mice) present a stable mII arrest (Dumont et al., 2005). Although it has recently been shown (Chang et al., 2009; Backs et al., 2010) that the γ isoform of CaMKII (CaMKIIγ) transmits the Ca^{2+} signal during mouse fertilization, the nature of this relay to Emi2 – whether, for example, it is direct – is unknown and mammalian Emi2 lacks the canonical $RXX^T/_S$ CaMKII phosphorylation target used in xEmi2 (Rauh et al., 2005; Perry and Verlhac, 2008).

Here, we report a detailed molecular dissection of mammalian Emi2 and mII arrest. *Xenopus* and mouse Emi2s are functionally non-equivalent. Both N- and C-terminal Emi2 domains possess metaphase modulating activity, the latter through a potential TSS phosphorylation, D-box, Zn^{2+}-binding motif and RL domain. Oocytes contain equimolar isoforms of CaMKIIγ, although neither directly phosphorylates Emi2 in vitro.

MATERIALS AND METHODS

Collection, culture and activation of oocytes

Eight- to 12-week-old B6D2F$_1$ females (SLC, Shizuoka-ken, Japan) were superovulated by standard serial intraperitoneal injection of pregnant mare serum gonadotropin (PMSG) followed 48 hours later by human chorionic gonadotropin (hCG). Oviductal mII oocytes were collected typically 12 to 14 hours after hCG injection and cumulus cells removed following hyaluronidase treatment as previously described (Yoshida et al., 2007; Suzuki et al., 2010). Fully grown germinal vesicle stage (GV) oocyte-cumulus cell complexes were collected from 8- to 10-week-old B6D2F$_1$ females 44 to 48 hours after PMSG injection. After 1 hour of culture in Waymouth medium (Waymouth, 1959) supplemented with 10% (v/v) foetal calf serum (FCS), cumulus cells were displaced from associated GV oocytes by repeated pipetting in TaM medium (Miki et al., 2006) supplemented with 10% FCS and 150 µM isobutylmethylxanthine (IBMX). GV oocytes were held in TaM medium containing 150 µM IBMX until micromanipulation and IBMX washed out or incubation in IBMX-containing medium continued, depending on the experiment (see Fig. S1

in the supplementary material). Culture of mII oocytes was typically in kalium simplex optimized medium (KSOM) (Erbach et al., 1994). All oocyte and embryo culture was in humidified CO_2 [5% (v/v) in air] at 37°C. Parthenogenetic activation was by incubating mII oocytes in Ca^{2+}-free CZB (Chatot et al., 1989) supplemented with 10 mM $SrCl_2$ in humidified CO_2 [5% (v/v) in air] at 37°C for 1 hour. Oocytes were then washed in KSOM and incubation continued at 37°C.

Sperm preparation and microinjection

Sperm were demembranated as described previously, with minor modifications (Yoshida et al., 2007). Briefly, cauda epididymidal spermatozoa from 12- to 30-week-old male B6D2F$_1$ mice were triturated in nuclear isolation medium [NIM: 125 mM KCl, 2.6 mM NaCl, 7.8 mM Na_2HPO_4, 1.4 mM KH_2PO_4, 3.0 mM EDTA (pH 7.45)] containing 1.0% (w/v) 3-[(3-cholamidopropyl)dimethylammonio]-1-propanesulfonate (CHAPS) at room temperature (25°C) for 1 minute and washed twice in ambient temperature NIM to give control demembranated heads – cHds. Where appropriate, sperm suspensions were incubated at 48°C for 30 minutes, with trituration after 15 minutes, to generate 'inactivated', iHd preparations. Sperm were mixed with 1 to 2 volumes of 15% (w/v) PVP$_{360}$ (average M_r=360,000; Kanto Chemical, Tokyo, Japan) and microinjected as described (Yoshida and Perry, 2007), typically within 60 minutes of PVP mixing.

Immunological methods

Standard immunoblotting (IB) was with rabbit polyclonal anti-CycB1 (Santa Cruz Biotechnology, CA, USA), anti-Emi2 (Shoji et al., 2006), anti-Tubγ (γ-tubulin; Abcam, MA, USA), rabbit monoclonal anti-phosphoErk1/2 (Cell Signaling Technology, MA, USA), rabbit polyclonal anti-MAPK1/2 (Cell Signaling), rabbit polyclonal anti-Mos (Santa Cruz), rabbit polyclonal anti-IP$_3$R (Calbiochem, USA), rabbit polyclonal anti-CaM (Zymed, CA, USA), rabbit polyclonal anti-Plk1 (Santa Cruz), goat polyclonal anti-CaMKIIγ (calmodulin kinase II γ; Santa Cruz), rabbit polyclonal anti-Cdc2 (Delta Biolabs, CA, USA), rabbit polyclonal anti-phosphoY15Cdc2 (R&D Systems, MN, USA) or rabbit polyclonal anti-Tuba (alpha-tubulin; Abcam) primary antibodies, and anti-rabbit or -goat IgG (Invitrogen) secondary antibodies.

Immune complex detection, IB of oocytes and early embryos, and immunoprecipitation (IP) from NIH 3T3 cell extracts, were performed essentially as described previously (Itoh et al., 1998; Shoji et al., 2006). NIH 3T3 cells were maintained in Dulbecco's modified Eagle's medium (DMEM, GIBCO) containing 10% (v/v) fetal bovine serum (FBS, Gemini-Bioscience) and penicillin/streptomycin (Sigma). Lipofectamine-mediated transfection (Invitrogen) of NIH 3T3 cells used 0.4 µg of each construct in pCI-Neo plasmid DNA (Shoji et al., 2006) per six-well plate. Constructs encoded bacterial alkaline phosphatase (BAP) or Emi2 (or deletions thereof) as C-terminal fusions to (FLAG)$_3$ for Fig. 4B, or mCherry (control) or Emi2-mCherry for Fig. 4F. Cells were collected 48 hours after transfection, and ~$5×10^6$ cells lysed in 300 µl incubation buffer [150 mM NaCl, 2 mM Na_2EDTA, 100 mM PMSF, 5 mM DTT, 50 mM Tris (pH 7.5)] supplemented with 0.05% (w/v) NP-40, on ice for 10 minutes. Where appropriate, TPEN was added to cells at a final concentration of 100 µM 1 hour prior to harvesting. Lysates were cleared by centrifugation at 20,000 ***g*** at 4°C for 30 minutes. Cleared lysates (~5%) were stored for analysis by SDS-PAGE, and

the remainder incubated with 20 µl of anti-Cdc27 (clone AF3.1, Sigma) or anti-DsRed (Clontech Laboratories, CA, USA) antibody overnight at 4°C and immunoprecipitates (IPs) incubated with protein A-agarose beads [12.5 µl of 50% (v/v) suspension] for 1 hour at 4°C, washed three times with ice-cold incubation buffer, and resuspended in a sample buffer. To generate FLAG IPs, lysates were applied to a mouse anti-FLAG M2 affinity matrix (Sigma) overnight with agitation at 4°C, unbound material removed, the matrix washed five times in 150 mM NaCl, 0.01% (v/v) NP-40, 10% (v/v) glycerol, and bound protein eluted at 4°C for 2 hours in a solution containing 5 mg/ml 3× FLAG peptide (Sigma) in 1 M NaCl, 0.5 M Tris (pH 7.5). Immunoblotting was with mouse anti-FLAG [1:1000 (v/v)] overnight and anti-mouse IgG secondary antibody [1:100,000 (v/v)] for 1 hour. Approximately 50% of each eluate was analyzed by SDS-PAGE. Labelled protein detection was performed as described previously (Shoji et al., 2006).

Preparation and injection of cRNA and siRNA
The different injection protocols adopted for in this work are illustrated in Fig. S1 in the supplementary material. Constructs containing PCR-generated Emi2 or Mos cDNA *Nhe*I-*Xho*I fragments cloned into pCI-Neo-mCherry (Shoji et al., 2006) were used to produce cRNA-encoded mCherry fusions at the C terminus of Emi2. Venus constructs were similarly constructed using a pCI-Neo-Venus scaffold, either as *Nhe*I-*Xho*I (β-Catenin) or *Nhe*I-*Xba*I (Emi2, Bora) fragments (see Fig. S11A in the supplementary material). For the transfections of Fig. 4B, (FLAG)₃-BAP or -Emi2 cDNA (i.e. encoding FLAG fused at the N terminus) were cloned into pNEBR-X1-Hygro (New England Biolabs, MA, USA) as *Xho*I-*Not*I fragments. For transfections in Fig. 4F, mCherry or Emi2-mCherry cDNA were cloned as *Xho*I-*Not*I fragments into pNEBR-X1-Hygro and the AAT preceding the start codon in Emi2-mCherry altered to ACC by site-directed mutagenesis. Site-directed mutagenesis was performed in the Quick-Change system (Stratagene, CA, USA). cRNAs were synthesized in vitro from linear plasmid DNA template and 5′-capped and polyadenylated in the same reaction using an mSCRIPT mRNA Production System (Epicentre Biotechnologies, WI, USA) according to the instructions of the manufacturer. cRNAs were dissolved in nuclease-free distilled water, quantified and stocked in aliquots at –80°C. Double-stranded siRNAs (iGENE Therapeutics, Tsukuba, Japan) were designed as described previously (Amanai et al., 2006) and stored in aliquots at –80°C.

RNA stock solutions were diluted with sterile DEPC-treated water to the desired concentration and 5~10 pl injected at default concentrations of 0.5 to 1.0 mg/ml ('Lo') or occasionally at higher concentrations (2.0 to 2.5 mg/ml; 'Hi') in Fig. 4G and Fig. S4 in the supplementary material, for cRNA and 25 µM for siRNA within 1 hour of thawing, either through a fine needle (tip inner diameter ≤1 µm) into GV oocytes in IBMX-containing M2 medium, or via a piezo-actuated micropipette (tip inner diameter 6~7 µm) into mII oocytes in M2 medium. Where appropriate, post-injection levels of cRNA were confirmed by semi-quantitative PCR (qPCR; not shown).

PCR
Ratiometric quantification of mRNAs (qPCR) was essentially as described previously, with cDNA prepared by Superscript (Invitrogen, CA, USA) from RNA from sperm or GV or mII oocytes (Amanai et al., 2006; Shoji et al., 2006) using the following primer pairs (5′ to 3′): *H2afz*, GCGTATCACCCCTCGTCACTTG and TCTTCTGTTGTCCT-TTCTTCCCG; *H3f3a*, CCATGCCAAACGTGTAACAA and TACCT-TTGACCCCATGGAAA; *mCherry*, TGAAGGTGACCAAGGGTGGC and AAGTAGTCGGGGATGTCGGC; *CaMKIIa,* AGCACCAAC-ACCACCATTGAGG and GGTCGCACATCTTCGTGTAGGACTC; *CaMKIIb*, TCTTCCGACAGCACCAACACAAC and GGGTCACAG-ATTTTCGCATAGGC; *CaMKIIg*, TGAGCCAGAAGCCCTTGGTAAC and GTTTAGGATGGTGGTGTGGATAGG; *CaMKIId*, TGGAAG-GGATGGACTTTCACAG and GAGCCGAATGTATGCGATGC; *CaM*, TCAGAACCCAACAGAAGCCG and TCCCATCCTTGTCAAAC-ACTCG. Data were normalized with respect to *H3f3a* or *H2afz*.

Enzyme inhibitors
To evaluate the role of CaN in mouse mII exit, oocytes were pre-incubated and injected in medium containing 100 µM FK506 (Sigma) and/or 2 µM cyclosporin A (CsA; Sigma) and incubation continued in inhibitor-containing medium. The CaN inhibitor peptide (iPep) ITSFEEAKGLDRINERMPPRRDAMP (Sigma) was co-injected with sperm at a pipette concentration of 500 µM. For sperm injection in the presence of inhibitors, sperm were pre-incubated in FK506 and/or CsA and/or iPep and injected so that the inhibitor concentrations were, respectively, 100, 200 or 500 µM within the pipette. Oocytes were scored for activation 5.25±0.25 hours after treatment in Fig. S8D. For the inhibition of calmodulin (CaM) and protein kinase C (PKC), oocytes were respectively incubated in media containing 100 µM CGS9343B (Sigma) or chelerythrine (Sigma) at the concentrations shown, each from 10 mM stocks in DMSO stored at –20°C. Where appropriate, preincubation was for 1 hour prior to SrCl₂ treatment and continued until reading.

Protein fluorescence imaging
Immunocytochemistry, differential interference contrast microscopy (DIC) and epifluorescence imaging were essentially as described previously (Yoshida et al., 2007). Images of live oocytes following cRNA injection were captured via a BioZero-8000 microscope/detector (Keyence, Osaka, Japan) and analyzed with BZ-Analyzer software (Keyence). Excitation at 540/25 nm was used with a TRITC (red) filter system for mCherry fluorescence detection and at 480/30 nm with a GFP (green) filter system to detect Venus epifluorescence.

Spindle behaviour during oocyte aging was visualized by time-lapse microscopy of transgenic oocytes containing a Venus-tubulin-alpha (Tuba) fusion protein whose expression was driven by the *ZP3* promoter on a C57BL/6 × C3H background (subsequently back-crossed to C57BL/6). The 4.5 kb *Bci*VI-*Mlu*I *pZP3→Venus-Tuba* transgene fragment was generated by inserting a 2019 bp *pZP3*-containing *Xho*I-*Kpn*I genomic DNA fragment upstream of a 710 bp *Bam*HI-*Bsr*GI *Venus* fragment linked to a 1633 bp *Bsr*GI-*Mlu*I fragment from pEGFP-Tuba, which encodes human tubulin-α (Clontech Laboratories, CA, USA). Oocytes were placed in a KSOM droplet under mineral oil on a glass-bottomed dish on the stage of a TE2000 inverted microscope (Nikon, Japan) equipped with a CSU10 confocal scanning unit (Yokogawa, Japan) and a humidified chamber [5% (v/v) CO₂ in air] at 37°C. DIC images and fluorescent (488 nm) images (typically 13 focal planes, step size=2 µm) were captured at 5-minute intervals by a C9100-13 ImagEM EM-CCD camera (Hamamatsu Photonics, Shizuoka, Japan) driven by MetaMorph (Molecular Devices, CA, USA) image analysis software.

Assays of protein kinase activity
H1 protein kinase assays of MPF activity for Fig. S2C in the supplementary material were as described previously (Shoji et al., 2006). For CaMKII phosphorylation assays, CAMKIIγ3, CaMKIIγJ, mouse Emi2 and xEmi2 were translated as Myc-His fusions in vitro using a TNT rapid coupled transcription/translation (IVTT) system (Promega) charged with 2 µg template DNA, and purified using the MagZ Protein Purification System (Promega, Cat. No. V8830). As a positive control, we employed preparation of bovine brain CaMKII containing all four isoforms (Upstate Biotechnology, NY, USA). CaMKII kinase assays were performed using the CaMKII Assay Kit (Upstate) as instructed by the manufacturers. Where appropriate, 9 µl of IVTT-purified mouse Emi2 or xEmi2 plus 1 µl of 400 ng/µl CaM replaced 10 µl CaMKII substrate cocktail (500 µM autocamtide peptide plus 40 ng/µl CaM). Where both autocamtide and Emi2 substrates were present in the same reaction, 10 µl of IVTT-purified (x)Emi2 and 10 µl of CaMKII substrate cocktail (500 µM autocamtide plus 40 ng/µl CaM) were added to give a final volume of 60 µl. As a negative control, ADBI buffer was included instead of CaMKII and/or Emi2. To visualize phosphorylation, 14 (out of 50) µl of each reaction was subjected to SDS-PAGE, fixed in a mixture of 30% (v/v) methanol plus 10% (v/v) acetic acid for 10 minutes, incubated in crack-proof solution for 10 minutes and dried prior to autoradiography using a BAS-2500 image detection system.

Computer methods
Student's *t*-tests were applied to comparative unpaired analyses. Data for each experiment were collected on at least 2 days. Emi2 protein sequences for mouse and species orthologues were obtained from Ensemble (http://www.ensemble.org/index/html) and the multiple alignments shown in Fig. 3A and Fig. 4C optimized via the CLUSTALW algorithm (http://align.genome.jp).
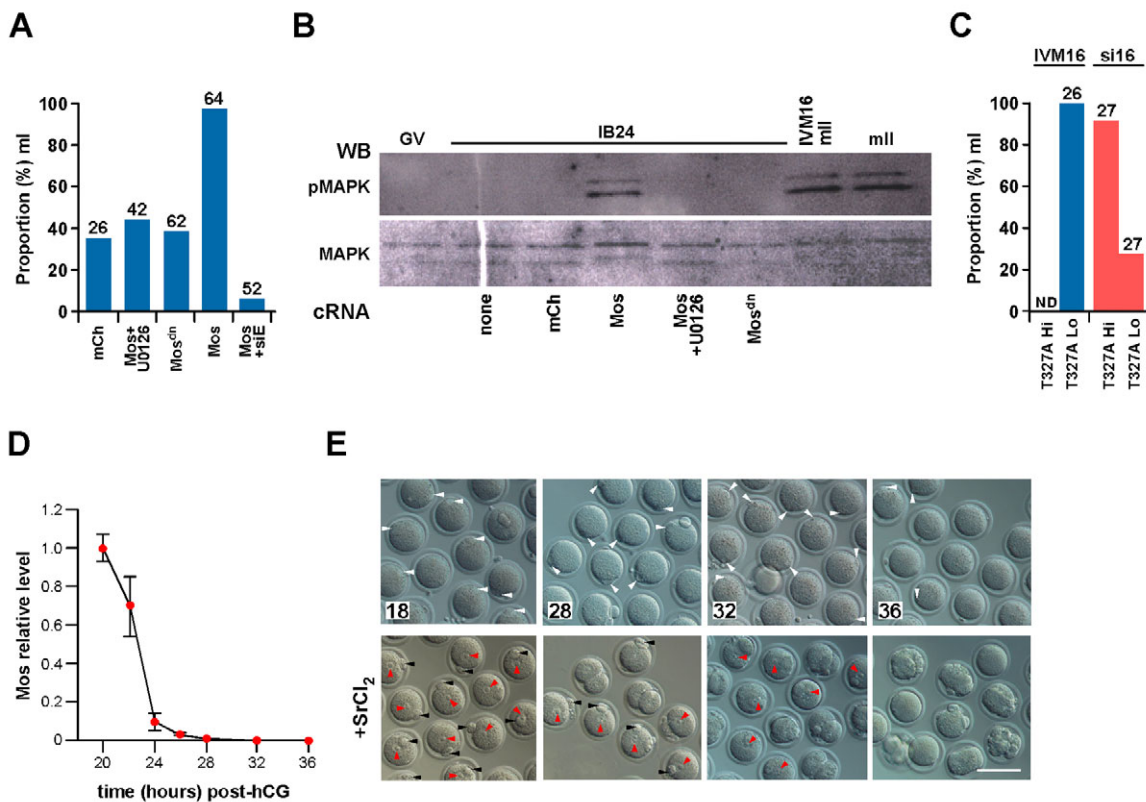
Fig. 2. Mos establishes Emi2- and MAPK-dependent metaphase arrest but its presence is not required to sustain mII. (**A**) Histograms for GV oocyte injection with cRNA encoding mCherry (mCh) or mCherry fused to Mos or to the Mos dominant-negative double mutant S3A/S105A (Mos^{dn}). Injections included the Mek inhibitor U0126 or *si5'Emi2#1* (Mos+siE), as indicated. Numbers above columns show oocyte numbers. (**B**) Anti-MAPK and -phospho-MAPK (pMAPK) immunoblotting of non-injected control IVM16, mII and GV oocytes or GV oocytes injected with cRNA as in A and held in IBMX (IB24) (see Fig. S1A in the supplementary material). Upper and lower panels show the same blot. (**C**) Percentages of oocytes arrested at mI in the IVM16 or si16 systems (see Fig. S1B,C in the supplementary material) following injection with cRNA encoding the Emi2^{T327A} (T327A). Lo, the default [cRNA] throughout (0.5-1.0 mg/ml); Hi, [RNA]=2.0-2.5 mg/ml. (**D**) Densitometric quantification of anti-Mos immunoblots of oocytes at the times shown post-hCG. See also Fig. S2C in the supplementary material. (**E**) Paired Hofmann images of mature oocytes at the ages indicated post-hCG (in hours), and (underneath) the same or equivalent oocytes 6 hours after exposure to 10 mM SrCl$_2$. Black arrowheads, Pb; red arrowheads, pronuclei; white arrowheads, protuberances caused by mII spindles/plates. Error bars indicate s.e.m. Scale bar: 100 μm.

RESULTS

Mos is required for Emi2 to establish, but not maintain mII arrest

In *Xenopus*, the classical cystostatic factor, xMos, stabilizes xEmi2 via xMAPK (Inoue et al., 2007), but roles for Mos in establishing and maintaining mII arrest in mammals have not been clearly delineated. To address this, we injected mouse germinal vesicle stage (GV) oocytes with complementary RNA (cRNA) encoding Mos-mCherry and cultured them for 24 hours in the phosphodiesterase inhibitor, IBMX, followed by in vitro maturation (IVM) for 16 hours (the IB24 protocol; see Fig. S1A in the supplementary material). Injected oocytes underwent 97.6±2.4% mI arrest, whereas the corresponding value dropped to 38.5±3.6% for the dominant-negative, Mos$^{S3A/S105A}$-mCherry and 35.7±14.3% for mCherry alone (Fig. 2A; see Fig. S2A in the supplementary material). Mos overexpression in IB24 oocytes induced the appearance of active, phospho-MAPK, but this was markedly reduced by the MAPKK (Mek) inhibitor U0126 (Fig. 2B), which also reduced the establishment of mI arrest by Mos (Fig. 2A). In corroborating earlier work relating Mos-MAPK to mouse cytostatic arrest (Verlhac et al., 1996), these findings confirm the fidelity of the IVM system.

The relationship between Mos and Emi2 in mammals was next investigated by co-injecting GV oocytes with *siEmi2* siRNA and *Mos-mCherry* cRNA in the IB24 system. Only 5.9±3.9% (*n*=52) of oocytes arrested at mI (Fig. 2A; see Fig. S2A in the supplementary material), suggesting that metaphase establishment by Mos requires Emi2. The *Xenopus* xMos-xMAPK pathway enhances xEmi2 stability and activity by phosphorylating S335 and T336 (Inoue et al., 2007). To test whether T336 of xEmi2 corresponds to T327 in the mouse, we injected *Emi2^{T327A}-mCherry* cRNA in the si16 system (see Fig. S1C in the supplementary material). High concentrations of Emi2^{T327A}-mCherry-encoding cRNA induced mI arrest (Fig. 2C), but only weakly compared with the same amount of cRNA encoding full-length Emi2-mCherry (compare Fig. 3D with 'T327A Lo' in Fig. 2C). This mirrors the result of a similar functional assay using xEmi2^{T336A} in *Xenopus* extracts (Inoue et al., 2007), consistent with an analogous role for T327 in mouse Emi2 to T336 in xEmi2.

Few data thus far distinguish between the role of Mos in the establishment versus the maintenance of mII arrest. We investigated this in aging oocytes, which from 18 to >36 hours post-hCG retained the morphological features of mII, although metaphase plate cortical protuberances eventually decreased in
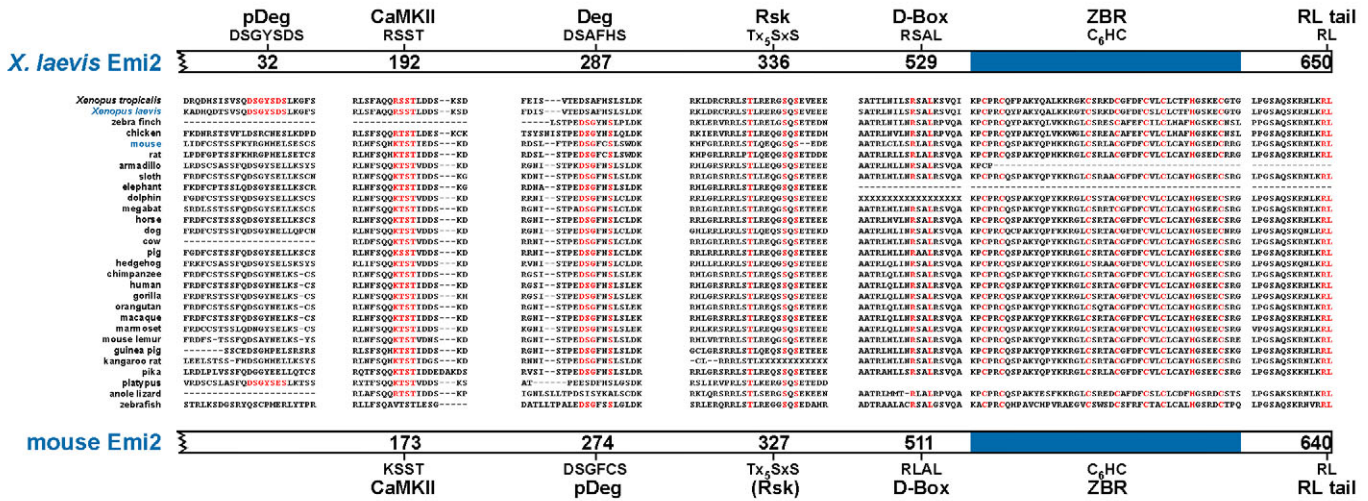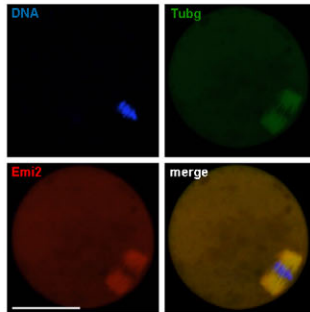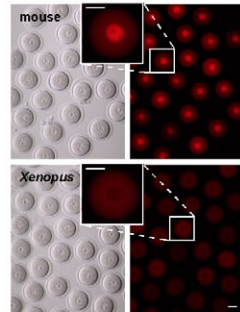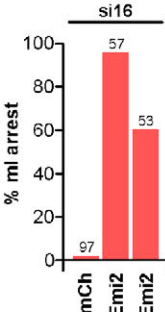
Fig. 3. Features of Emi2 species orthologues. (**A**) Optimized alignment of regions of Emi2 from different species showing positional correspondence to functional domains and residues (red) in *Xenopus laevis* xEmi2. (p)Deg, (phospho)degron. (**B**) Fluorescence images after GV oocyte injection with cRNA encoding Emi2-mCherry in the IVM16 system (see Fig. S1B in the supplementary material), showing Emi2 spindle localization. Tubg, γ-Tubulin. DNA is stained with DAPI. (**C**) GV oocytes injected with cRNA encoding full-length mouse or *Xenopus* Emi2 and held for 5 hours in IBMX prior to visualization. Insets show Emi2 nuclear localization in mouse, but not in *Xenopus*. (**D**) Percentages of mI arrest following GV oocyte injection with cRNA encoding mCherry (mCh), Emi2 or xEmi2 in the si16 system (see Fig. S1C in the supplementary material). Scale bars: 50 μm.

size and number (Fig. 2E). The spindles of *Venus-tuba* transgene-expressing mII oocytes elongated and occasionally became decoupled from the cortex during aging (see Fig. S2B in the supplementary material) (Webb et al., 1986). Immunoblotting showed that levels of meiotic exit signalling proteins changed little; phospho-MAPK exhibited a pronounced decline after only 32 hours, the inactive Cdc2 modification Y15-phospho-Cdc2 was undetectable, and H1 kinase activity, a marker of MPF (i.e. mII) persisted (see Fig. S2C in the supplementary material). By contrast, Mos levels declined markedly and were undetectable by ~28 hours post-hCG (Fig. 2D; see Fig. S2C in the supplementary material). Exposure to the parthenogenetic agent, SrCl$_2$ activated >95% of oocytes up to 32 hours post-hCG, and ~50% thereafter. The proportion undergoing aberrant cytokinesis following SrCl$_2$ treatment exhibited a pronounced increase after 32 hours (Fig. 2E).

These findings suggest that Mos is not sufficient in itself to establish mouse meiotic metaphase but requires Emi2, to which it signals via MAPK. The disappearance of Mos during mII oocyte

aging correlates with aberrant spindle behaviour in oocytes that are competent to exit mII, indicating that Mos is not required for mII maintenance.

Xenopus and mouse Emi2s are not interchangeable

These results raise the possibility that mammalian and *Xenopus* Emi2s are also functionally distinct. Species alignment of predicted Emi2 sequences conserves multiple regulatory elements of xEmi2 (Fig. 3A) but it is not known whether they function outside *Xenopus*. To address this, we compared xEmi2 and mouse Emi2 behaviour in mouse oocytes.

Mouse GV oocytes were injected with cRNA encoding mCherry and subjected to IVM for 16 hours (referred to as IVM16; see Fig. S1B in the supplementary material). Of these *mCherry*-injected controls, 90±1.9% (*n*=61) underwent normal meiotic progression and arrested at mII, whereas those injected with *Emi2-mCherry* cRNA precociously arrested at mI (see Fig. S3A in the supplementary material). Emi2 localized to mI spindles (Fig. 3B);

no first polar body (Pb_1) extrusion was observed by videomicroscopy (not shown). Segments of Emi2 (residues 1-250 and 251-C-terminus) localized nebulously to spindles (see Fig. S3B in the supplementary material). When GV (i.e. nuclear) breakdown was suspended by IBMX, Emi2-mCherry was efficiently targeted to the GV, localizing to a nuclear domain outside the nucleolus-like body (Bouniol-Baly et al., 1999; Fig. 3C; see Fig. S3C in the supplementary material) and to nuclei in NIH 3T3 cells (not shown), even though Emi2 lacks a consensus nuclear localization motif (Lee et al., 2006). Similar GV localization was exhibited by $Emi2_{251\text{-}C\text{-}ter}$ – but not by the N-terminal Emi2 domain of $Emi2_{1\text{-}250}$-mCherry (see Fig. S3C in the supplementary material).

These experiments did not distinguish between the metaphase-imposing activities of Emi2-mCherry and native Emi2. To address this, we employed the si16 system of RNAi (see Fig. S1C in the supplementary material) to deplete native Emi2, by injecting *siEmi2-5′UTR#1* (Fig. 3D; see Fig. S3D in the supplementary material) or *#2* (not shown), which are specific to native *Emi2* mRNA (Shoji et al., 2006; Amanai et al., 2006). As expected (Shoji et al., 2006), almost none (1.9±1.9%) of the oocytes injected with *mCherry* cRNA in the si16 system established mI arrest, whereas mouse *Emi2-mCherry* cRNA caused 95.6±2.6% mI arrest (Fig. 3D), showing that the Emi2 knock-down phenotype had been rescued.

If xEmi2 is mechanistically equivalent to mouse Emi2, it should have similar properties. However, in contrast to Emi2, xEmi2-mCherry was excluded from the GV of IBMX-treated oocytes, suggesting that it lacked a nuclear targeting signal (Fig. 3C). When native Emi2 was depleted in the si16 system, xEmi2-mCherry elicited metaphase (mI and mII) at a lower efficiency than that achieved by its mouse counterpart, Emi2-mCherry (Fig. 3D; see Fig. S3D in the supplementary material). These findings indicate that mouse and *Xenopus* Emi2s are not functionally interchangeable and that they participate in distinct regulatory mechanisms. We therefore sought a mechanistic dissection of mouse Emi2 in vivo.

A regulatory N-terminal domain complements the principal zinc-dependent C-terminal cytostatic activity of mouse Emi2

Injecting GV oocytes with cRNA encoding either $Emi2_{1\text{-}250}$ or $Emi2_{251\text{-}Cter}$ as mCherry fusions induced ~100% mI arrest following IVM16 in a manner analogous to full-length Emi2-mCherry (Fig. 4A; see Fig. S4 in the supplementary material). Analogous to xEmi2, functional MAPK-dependent phosphorylation, D-box and ZBR motifs all reside in $Emi2_{251\text{-}Cter}$ (Fig. 3A), so $Emi2_{1\text{-}250}$ was not expected to possess cytostatic activity. In mitotic cells, full-length Emi2 and $Emi2_{251\text{-}Cter}$ co-complexed with APC subunits Cdc20 and Cdc27, as judged by co-immunoprecipitation (Fig. 4B). We did not observe interactions between $Emi2_{1\text{-}250}$ and Cdc27, but occasionally detected an interaction between $Emi2_{1\text{-}250}$ and Cdc20 (Fig. 4B). $Emi2_{251\text{-}Cter}$ retained the ability to induce mI arrest in si16 oocytes but $Emi2_{1\text{-}250}$ did not (Fig. 4A; see Fig. S4 in the supplementary material), suggesting mechanisms that are, respectively, independent of and dependent on native Emi2.

We wished to define more specifically the Emi2 N-terminal cytostatic function. Residues 1-100 induced mI arrest in 42.3±3.6% (*n*=26) of IVM16 oocytes (Fig. 4A), suggesting that residue 100 lies within the cytostatic N-terminal region. Consistent with this, $Emi2_{80\text{-}115}$ induced 100% IVM16 mI arrest, but did not in si16 oocytes (Fig. 4A; see Fig. S4 in the supplementary material). Residues 80-115 of ectopically expressed Emi2 are therefore not

inherently sufficient for metaphase establishment but enhance native Emi2-dependent mI arrest; the region is conserved among mammals (Fig. 4C).

The Emi2 C terminus contains a putative ZBR, but although a single ZBR mutant of *Xenopus* xEmi2 lacked cytostatic activity in cell-free extracts, its stability was not reported (Schmidt et al., 2005). To address the relationship between Emi2 and Zn^{2+} in mII maintenance, we injected mII oocytes with cRNA and exposed them ~4 hours later to the highly specific Zn^{2+} chelator, *N,N,N′,N′*-tetrakis-(2-pyridylmethyl)-ethylenediamine (TPEN), which has been shown to induce meiotic exit (Suzuki et al., 2010). Injection with cRNA encoding Emi2-mCherry, but not mCherry or $Emi2^{C573A}$-mCherry (a mutant within its putative ZBR; see below), reduced the efficiency of TPEN-induced mII exit (Pb_2 extrusion; Fig. 4D). Injection of cRNA encoding ZBR mutants in the si16 system generally produced mCherry fluorescence intensities lower than Emi2-mCherry controls (see Fig. S5 in the supplementary material), even though qPCR confirmed higher mutant [cRNA] in oocytes (average, 1.23±0.38; control [*Emi2-mCherry*]=1.0±0.0). To compensate, more cRNA was injected and the resultant mCherry epifluorescence level related to its corresponding ability to impose metaphase arrest (Fig. 4E; see Fig. S6 in the supplementary material). These experiments indicate a pronounced contribution from ZBR residues C573, C591, C601 to Emi2 cytostatic activity in vivo.

Pre-treatment with TPEN had no discernable effect on Emi2 complex formation with the APC core subunit, Cdc27 in NIH 3T3 cells (Fig. 4F), consistent with separable APC- and Zn^{2+}-binding domains (Miller et al., 2006; Tang et al., 2010). We also found that whereas $Emi2_{551\text{-}Cter}$ was unable to impose metaphase arrest in si16 oocytes, $Emi2_{491\text{-}Cter}$ did so efficiently; the results were mirrored in the IVM16 system (Fig. 4G; see Fig. S7A in the supplementary material). This lead us to investigate the candidate D-box RXXL, which lies between 491 and 551. The double mutant $Emi2^{R511A,L514A}$-mCherry induced mI arrest only weakly in si16 oocytes (22.5±2.5%, *n*=29), even when expressed at high levels (Fig. 4G; see Fig. S7A in the supplementary material), indicating that R511 and/or L514 are required by Emi2-mCherry for full cytostatic activity.

These studies predict autonomous meiotic regulatory activity in the Emi2 C terminus. Indeed, when cRNA encoding $Emi2_{551\text{-}Cter}$ was injected into mII oocytes, ~100% underwent meiotic exit (Fig. 4H; see Fig. S7B in the supplementary material). This was probably not due to Zn^{2+} sequestration by the ZBR, as $Emi2_{551\text{-}Cter}^{C573A}$ also efficiently induced meiotic exit (Fig. 4H). Recently, an RL domain at the C terminus has been shown in *Xenopus* to mediate APC binding (Ohe et al., 2010). Accordingly, cRNA encoding $Emi2_{551\text{-}Cter}^{\Delta RL}$, in which the RL domain had been deleted, failed to elicit mII exit (Fig. 4H). However, $Emi2_{491\text{-}Cter}$, which contains the RLAL D-box in addition to the ZBR and RL domain (Fig. 3A), only modestly (13.3±13.3%, *n*=30) induced mII exit (Fig. 4H), suggesting that it contained information not present in $Emi2_{551\text{-}Cter}$ that tended to impose mII.

Collectively, these data support the conclusion that residues 491 to the C terminus represent the (near) minimal region of Emi2 required for it to establish and maintain metaphase arrest. Meiotic stabilization by Emi2 involves its D-box (residues 511-514), ZBR (573~613) and RL domain (640-641) and possibly an indirect mechanism involving a novel N-terminal domain (80-115).
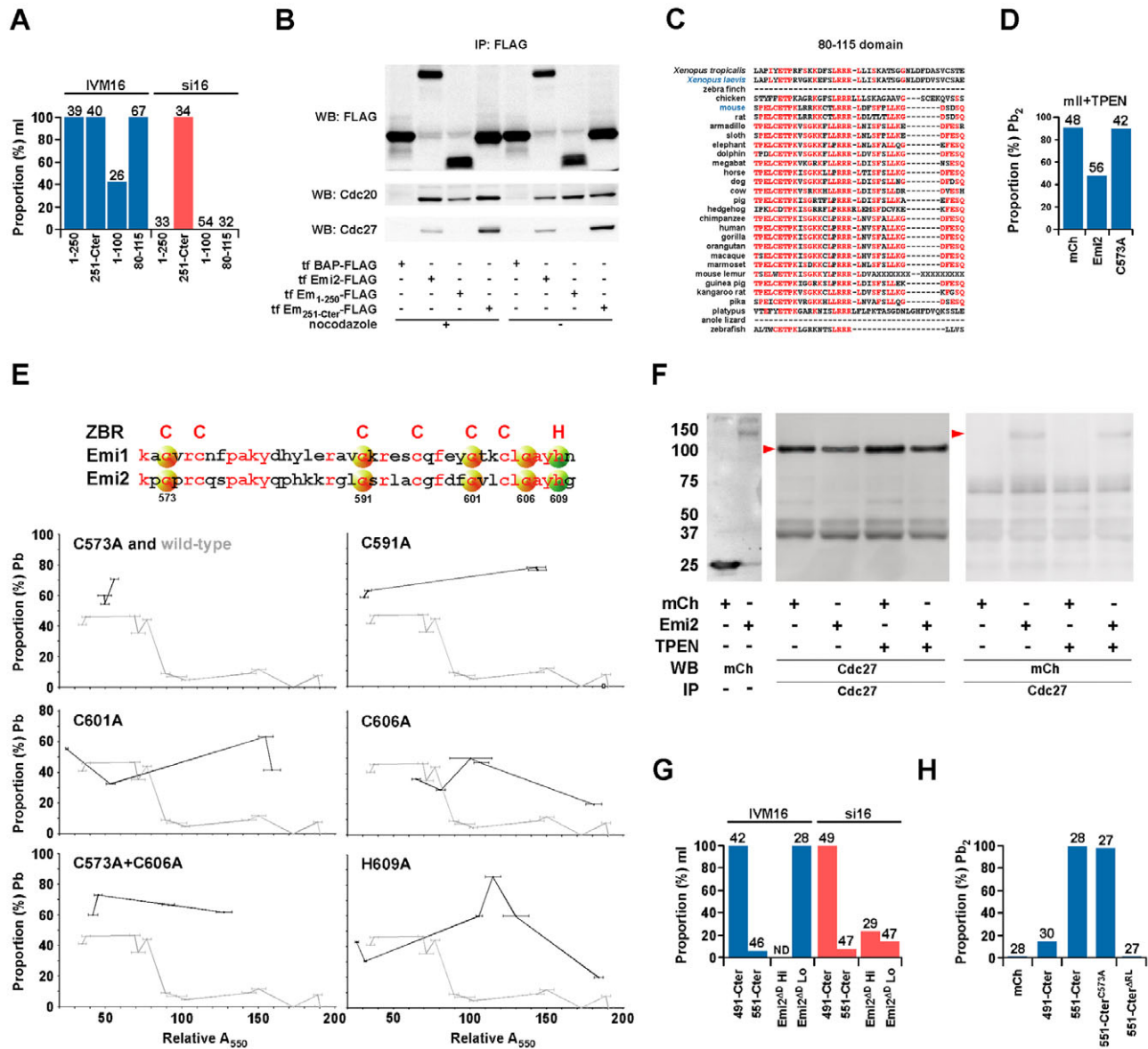
Fig. 4. Mouse Emi2 comprises separable functional domains. (**A**) Percentages of oocytes arrested at mI in the IVM16 or si16 systems (see Fig. S1B,C in the supplementary material) following injection with cRNAs encoding different Emi2 constructs. Values below the *x*-axis correspond to Emi2 residue numbers. (**B**) Immunoblotting of lysates from NIH 3T3 cells transfected (tf) as indicated, in the presence or absence of nocodazole, and subjected to anti-FLAG immunoprecipitation (IP) with beads to capture complexes containing FLAG (uppermost), or endogenous Cdc20 (centre) or Cdc27. (**C**) Optimal species alignment with mouse Emi2 residues 80-115. Residues that are identical in more than 50% of the sequences are shown in red. (**D**) Intact mII oocytes were injected with cRNA encoding mCherry (mCh), Emi2-mCherry or Emi2^{C573A} (C573A), exposed to TPEN (10 μM) after 4 hours then scored for Pb$_2$ extrusion 1.5 hours later. (**E**) Alignment of parts of mouse Emi1 and Emi2 (with Emi2 residue numbering) ZBRs. Varying [cRNA] encoding Emi2 mutants were injected in the si16 system, and fluorescence quantified (*x*-axis) and plotted against the proportion emitting a Pb (average 14.8 oocytes/point). The wild-type Emi2 profile is shown on each plot for comparison (grey). (**F**) Western blotting of lysates from NIH 3T3 cells transfected with mCherry or Emi2-mCherry (Emi2) (leftmost) and following IP to capture endogenous Cdc27. Red arrowheads mark complexes containing Cdc27 (left) and Emi2-mCherry. Cells were incubated in 100 μM TPEN prior to collection as indicated. (**G**) cRNAs encoding Emi2$_{491-Cter}$ (491-Cter), Emi2$_{551-Cter}$ (551-Cter) or Emi2^{ΔD} (D-box double mutant, R511A, L514A) injected in the IVM16 or si16 systems, showing the percentage arrested at mI. Low (Lo) and high (Hi) RNA concentration are, respectively, 0.5-1.0 and 2.0-2.5 mg/ml; the Lo value corresponds to the default used in other experiments. (**H**) Mature mII oocytes injected with cRNA encoding mCherry (mCh), Emi2$_{491-Cter}$ (491-Cter), or Emi2$_{551-Cter}$ (551-Cter) or Emi2$_{551-Cter}$ containing the mutations indicated were scored for mII exit as indicated by Pb$_2$ emission 2 hours post-injection. Values above columns show oocyte numbers. Emi2 constructs were all expressed as mCherry fusions.

The regulation of metaphase exit and Emi2 degradation

We next investigated signalling processes implicated in mII exit to test how they converged on Emi2. The calmodulin (CaM) inhibitor, CGS9343B inhibited Pb$_2$ emission and ectopic Emi2 degradation

following parthenogenetic activation (see Fig. S8A,B in the supplementary material). CaM-dependent enzymes calcineurin (CaN, also called PP2B) and calmodulin kinase II (CaMKII) mediate *Xenopus* mII exit and it has been suggested that they achieve this by regulating xEmi2 degradation (Rauh et al., 2005;
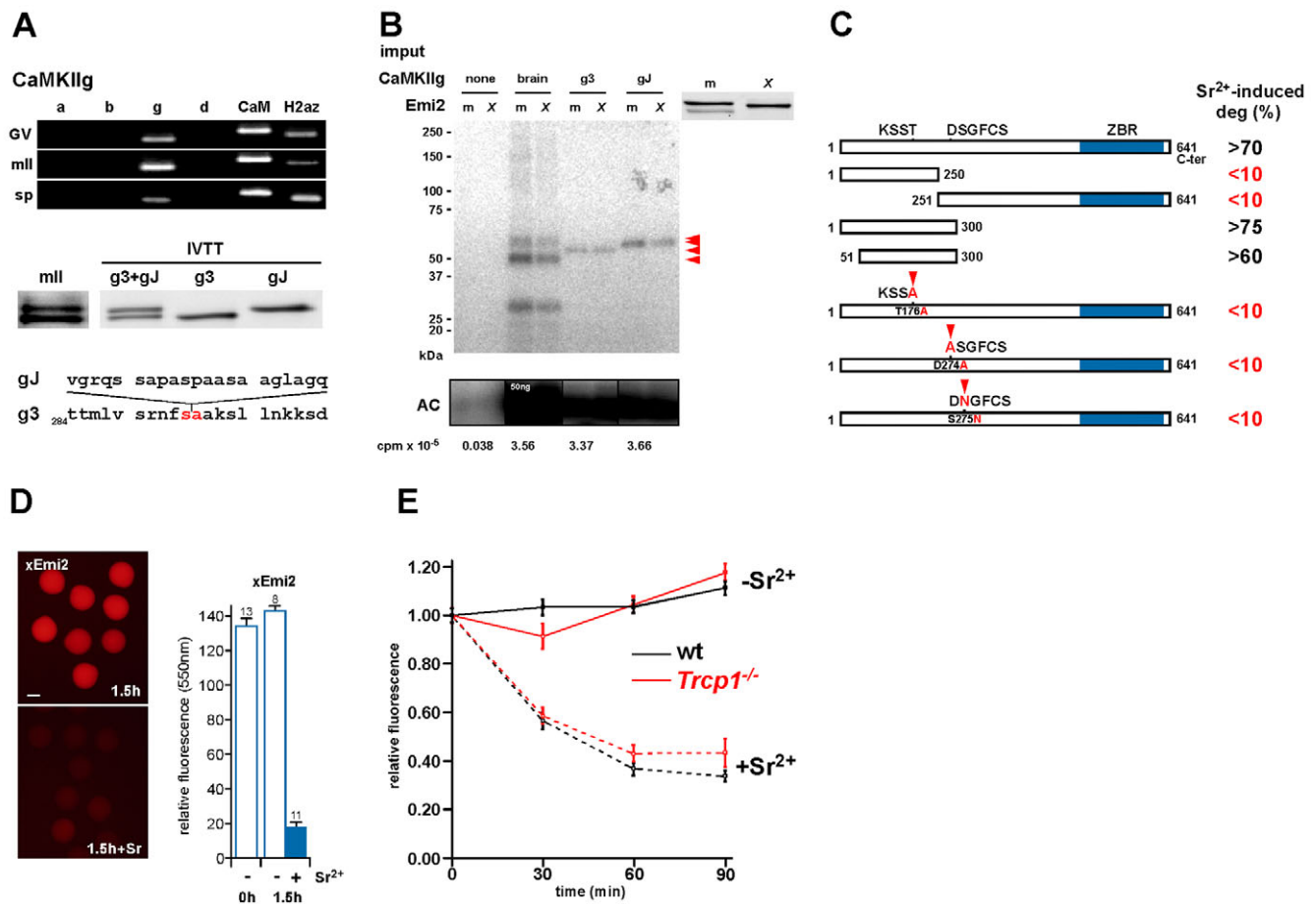
Fig. 5. Molecular regulation of mII exit by Emi2. (**A**) Agarose gel electrophoresis of RT-PCR (top) detects transcripts for CaM and the CaMKII γ isoform (g), but not α, β or δ (a, b and g) in sperm (sp) or oocytes (GV and mII). Immunoblotting (centre) with anti-CaMKIIγ reveals two isoforms, γ3 and γJ, in mII oocytes, the variant sequences of which are shown below. IVTT, coupled in vitro transcription/translation. (**B**) SDS-PAGE of in vitro assays to measure phosphorylation of mouse Emi2 (m) and xEmi2 (X) produced in vitro, by CaMKIIγ mII oocyte isoforms (γ3 and γJ) produced in vitro (A) or a mixture of all CaMKII isoforms from bovine brain (brain). AC, positive control autocamtide peptide. Red arrowheads indicate autophosphorylated CaMKII monomers. (**C**) Data summary of ectopic Emi2 degradation following oocyte activation. mII oocytes injected with cRNA encoding mCherry fused to Emi2, or the Emi2 mutations indicated were exposed to 10 mM $SrCl_2$ (see Fig. S1D in the supplementary material) and fluorescence levels recorded 1 hour after $SrCl_2$ withdrawal. Complete data sets are presented in Fig. S10A,B in the supplementary material. (**D**) Fluorescence images (left) and histograms for mII oocytes injected with cRNA encoding xEmi2-mCherry (xEmi2), without (top) or with exposure to $SrCl_2$ as in C. Recordings were made at the times indicated after oocytes had been exposed to $SrCl_2$ for 1.5 hours. Scale bar: 50 μm. Values above columns show oocyte numbers. (**E**) Fluorescence levels in mII oocytes injected with cRNA encoding Emi2-mCherry and 4 hours later treated with 10 mM $SrCl_2$ (+Sr^{2+}, broken lines) or not treated (–Sr^{2+}, solid lines). Oocytes were from the hybrid B6D2F$_1$ (black plots, wt) or homozygous null $Trcpb1^{-/-}$ mutants (red).

Nishiyama et al., 2007b). However, mouse oocytes lacked the CaN catalytic A subunit above a detection limit of ~700 fg/oocyte (43 nM; see Fig. S8C in the supplementary material), 10- to 100-fold lower than CaN concentrations in other tissues (Sharma et al., 1979; Stewart et al., 1983). ICSI-induced mII exit was slowed but not prevented by a combination of the CaN inhibitors CsA, FK506 or CaN-inhibitory peptide (see Fig. S8D in the supplementary material). Thus, in contrast to *Xenopus*, we found no evidence that CaN is essential for mouse mII exit, suggesting that the principal effect of CGS9343B was indirectly to reduce CaMKII activity.

In keeping with recent reports (Chang et al., 2009; Backs et al., 2010), GV and mII oocytes contained mRNA for CaMKIIγ (CaMKIIγ) but not the three other isoforms; we also found CaMKIIγ transcripts in spermatozoa (Fig. 5A). Mature mII oocytes contained two *CaMKIIγ* mRNA variants, encoding the previously reported 67 kDa γ3 (γ3) isoform (Chang et al., 2009) and the J isoform (γJ), not previously described in the mouse, containing a

predicted 21 amino acid variable domain insertion (AAL69956.1; Fig. 5A) (Gangopadhyay et al., 2003). CaMKIIγ3 and γJ isoforms were approximately equimolar in mII oocytes (Fig. 5A).

Injecting a mixture of active bovine brain CaMKII isoforms into mII oocytes did not induce mII exit (not shown), leading us to challenge *Xenopus* and mouse (x)Emi2 proteins with active bovine brain CaMKIIγ or mouse oocyte CaMKIIγ3 and γJ isoforms in a phosphorylation assay in vitro. All CaMKII preparations tested phosphorylated a control substrate and exhibited autophosphorylation, indicative of holoenzyme activity (Fig. 5B). However, there was little or no phosphorylation of either mouse or *Xenopus* (x)Emi2 (Fig. 5B). The absence of detectable Emi2 phosphorylation in vitro is unlikely to be because CaMKII functions as a non-CaMKIIγ hetero-multimer, as neither was phosphorylated by the cocktail of neuronal CaMKII isoforms (Fig. 5B). We therefore investigated whether this lack of phosphorylation in vitro might reflect a predisposing requirement for protein kinase
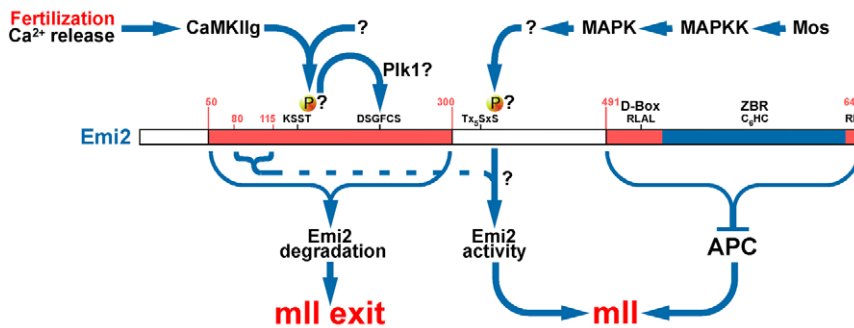
Fig. 6. Mouse Emi2 as meiotic regulatory hub. Diagram showing interactions between principal components of mouse meiotic homeostasis and Emi2. APC, anaphase-promoting complex; CaMKIIg, calmodulin kinase II γ; D-box, destruction box; Emi2, endogenous meiotic inhibitor 2; MAPK, mitogen-activated protein (MAP) kinase; MAPKK, MAP kinase kinase; Mos, Moloney sarcoma oncogene; Plk1, polo-like kinase 1; ZBR, zinc-binding region. A broken line shows a presumptive, possibly indirect, stabilization role for Emi2 residues 80-115. There is no evidence for the indispensable involvement of CaN.

C (PKC), which has also been implicated in oocyte activation (Halet, 2004). Combining CGS9343B with the PKC inhibitor chelerythrine markedly inhibited mII exit (see Fig. S8E in the supplementary material), but chelerythrine alone only modestly inhibited Emi2-mCherry degradation in mII oocytes (see Fig. S8F in the supplementary material) suggesting that PKC does not potentiate CaMKIIγ signalling that might lead to Emi2 degradation.

To address whether CaMKII transduces the Ca^{2+} signal at fertilization to degrade mouse Emi2, mature mII oocytes were injected with cRNA encoding truncation mutant Emi2 mCherry fusions, followed by Sr^{2+} exposure [mII(Sr)] or ICSI [mII(ICSI); see Fig. S1D,E in the supplementary material]. Taking fluorescence decrease as a meter of degradation, Sr^{2+} induced loss of $Emi2_{1-300}$- and $Emi2_{50-300}$-, but not $Emi2_{1-250}$- or $Emi2_{251-Cter}$-mCherry (Fig. 5C; see Fig. S9, S10 in the supplementary material). Thus, residues 50-300 are apparently required for Ca^{2+}-dependent degradation of mouse Emi2, but not the region corresponding to the Plx N-terminal phosphodegron in xEmi2 (Fig. 3A). Analogous to *Xenopus*, residues 50-300 contain a candidate, non-canonical CaMKII phosphorylation target, T176 (Fig. 3A); full-length xEmi2 was efficiently degraded in response to Sr^{2+} in mouse oocytes (Fig. 5D). Mouse $Emi2^{T176A}$-mCherry did not undergo Sr^{2+}-induced degradation in mII oocytes (Fig. 5C). A similar phenotype was exhibited by D274A and S275N mutants, which lay within a consensus phosphodegron, $DSGX_nS$ (Fig. 5C); the corresponding phosphodegron is located differently in xEmi2, and is essential for destruction downstream of Ca^{2+}-dependent xCaMKII phosphorylation (Rauh et al., 2005).

Finally, we investigated the activity responsible for Emi2 removal in response to fertilization-induced Ca^{2+} mobilization. The degradation of Emi2 is highly selective in that Ca^{2+} mobilization does not result in the targeting of Ca^{2+}/Plk1-regulated substrates, Emi1, β-Catenin or Bora for destruction (see Fig. S10, Fig. S11A in the supplementary material). The pathway responsible did not require the APC, as depletion of its activator, Cdc20, by RNAi (Amanai et al., 2006) had little, if any, effect on Emi2 degradation (see Fig. S11B in the supplementary material). Moreover, degradation of Emi2 occurred efficiently in the oocytes of gene-targeted mice lacking the E3 ubiquitin ligase SCF component Trcpb1 (Fig. 5E), implying that Trcpb1 is not essential.

DISCUSSION

This work reveals in intact mouse oocytes, essential domains and residues, protein interactions and degradative mechanisms required by Emi2 to establish, maintain and exit from meiotic metaphase (Fig. 6). We also show that the establishment of metaphase by Mos requires Emi2 and suggest that they are linked by MAPK, as in *Xenopus* (Inoue et al., 2007). This begs the question of precisely

how, as *Xenopus* MAPK signals to xEmi2 via xRsk, but Rsk is dispensable in the mouse (Dumont et al., 2005). It was therefore important to establish whether mouse Emi2 possessed a functional site corresponding to the *Xenopus* xRsk phosphorylation target. It does: T327 (which corresponds to the xRsk target, T336 in *Xenopus*) is essential for mouse Emi2 cytostatic activity. This suggests that Mos-MAPK signals to Emi2 either directly or via a similar pathway to that in *Xenopus*, omitting Rsk and passing through an unknown intermediate.

Our work implies that, once established, Mos is not required to maintain mammalian mII in that it autonomously disappears during mouse mII oocyte aging. Rather, the disappearance of Mos occurs during an increase in spindle abnormalities (Webb et al., 1986; Verlhac et al., 1996) (Fig. 2). Loss of active MAPK also correlates with spindle lengthening (see Fig. S2B,C in the supplementary material), implicating the mouse oocyte spindle regulators MISS and Doc1R, both of which are MAPK substrates that do not mediate mII arrest (Lefebvre et al., 2002; Terret et al., 2003). It is therefore possible that, after mII arrest is established, the principal role of Mos is to maintain spindle integrity, possibly in conjunction with spindle regulators such as MISS and Doc1R.

Mouse Emi2 and *Xenopus* xEmi2 possess distinguishable activities in mouse oocytes; xEmi2 did not fully compensate for mouse Emi2 in meiotic regulation and localization patterns of xEmi2 were different from those of mouse Emi2. Differences may (in part) reflect the temperatures at which mouse and *Xenopus* fertilization occurs: 36.9°C and ~23°C, respectively. Species alignment of Emi2 sequences reveals both conservation and variation of domains and amino acid residues shown to be important for xEmi2 function (Fig. 3A), suggesting that non-conserved regions have evolved in different species to perform these functions.

It has already been shown that mouse Emi2 has the ability to arrest meiotic oocytes at metaphase (Shoji et al., 2006). When expressed in GV oocytes, this cytostatic activity was found principally to reside in a large C-terminal segment ($Emi2_{251-Cter}$), which contains domains that are important for Emi2 regulation by analogy to *Xenopus*, including PP2A-interacting domains, a D-box, ZBR and RL domain (Fig. 3A) (Schmidt et al., 2005; Wu et al., 2007a; Nishiyama et al., 2007a; Ohe et al., 2010). We provide evidence here and in complementary work (Suzuki et al., 2010), that Zn^{2+} is required for mII arrest, working through Emi2; we identify residues that contribute to the putative Zn^{2+}-coordinating lattice needed for Emi2 cytostatic activity. Taken together, these results suggest that a Zn^{2+}-containing functional Emi2 ZBR is essential for it to inhibit the APC in vivo.

A fragment of Emi2 from 551-Cter elicited mII exit with or without the ZBR mutation, C573A (Fig. 4H; see Fig. S7B in the supplementary material). This fragment contains a C-terminal RL

motif shown in *Xenopus* to mediate Emi2-APC binding, the over-expression of which causes native Emi2 to dissociate from the APC, causing meiotic progression (Ohe et al., 2010). A similar mechanism is likely in the mouse, as $Emi2_{551-Cter}^{\Delta RL}$ failed to induce mII exit (Fig. 4H). In contrast to 551-Cter, Emi2 residues 491-Cter, which also contain the D-box and RLAL, only weakly induced mII exit (Fig. 4H). The low activity relative to 551-Cter is probably not because the D-box turned the fragment into an APC substrate; expression levels were comparably high (see Fig. S7B in the supplementary material). Rather, we favour a model in which the D-box, when combined with ZBR and RL domains, effectively inhibits the APC, consistent with the behaviour of xEmi2 (Tang et al., 2010). We tested this in the IVM16 and si16 systems and found that, unlike $Emi2_{551-Cter}$, which possessed only limited cytostatic activity, $Emi2_{491-Cter}$ was sufficient for potent metaphase establishment and maintenance (Fig. 4G; see Fig. S7A in the supplementary material). This is in keeping with the situation in *Xenopus* (Wu et al., 2007b; Tang et al., 2010) and indicates that in mammals a region of Emi2 from a position between residues 491 and 551 to the C terminus is sufficient to establish and maintain mII arrest.

Unexpectedly, an N-terminal fragment, $Emi2_{1-250}$, also exhibited metaphase-inducing activity, as evidenced by its ability to impose mI arrest in GV oocytes (Fig. 4A; see Fig. S4 in the supplementary material). This activity required native Emi2, implying an indirect mechanism. Deletion mutagenesis mapped the activity to a region (residues 80-115) that lacks consensus phosphorylation or other regulatory sites (Marchler-Bauer et al., 2009) but is conserved among several species, including mammals (Fig. 4C). It has been suggested (Wu and Kornbluth, 2008) that smooth mI-to-mII transition relies on Emi2 degradation in mI, and it is possible that $Emi2_{80-115}$ is required for mI inactivation and/or degradation of Emi2, such that ectopically expressed 80-115 interferes with this negative regulation.

Separable modules of mouse Emi2 orchestrate mII metaphase establishment and exit. In *Xenopus*, it has been shown that S33/38 is essential for xEmi2 degradation during mII exit, but although there are signs that this degron (DSGX$_n$S) is conserved in lizards and the platypus, there is no conserved motif in the N-terminal region of Emi2 from most other species, including eutherian mammals (Fig. 3A). *Xenopus* possesses the more C-terminal sequence, DSAFHS, that is involved in degradation independently of mII exit (Nishiyama et al., 2007a) and this position corresponds to $^{274}DSGFCS^{279}$ in the mouse; we find that D274 and S275 are essential for Ca^{2+}-dependent mouse Emi2 degradation (Fig. 5C; see Fig. S10B in the supplementary material). Consistent with this, the $^{274}DSGFCS^{279}$ motif is located among residues 51-300, which approximately define the minimal region of Emi2 sufficient for Ca^{2+}-dependent degradation (Fig. 5C). This suggests that the motif has become a Ca^{2+}-dependent phosphodegron in the mouse and other species in which it is conserved (Fig. 3A) and that the position of this Emi2 phosphodegron has shifted during evolution. The reasons for this transposition will remain unknown until the function of the N-terminal domain of Emi2 becomes clear. The evolutionary retention of an N-terminal extension in mammals, even though it is no longer required for mII exit, implies that it plays one or more additional roles, such as that played by residues 80-115 or even roles that do not directly modulate the cell cycle.

We found no evidence that CaN is essential for mII exit in the mouse: a cocktail of inhibitors did not prevent meiotic exit and the CaN catalytic subunit was undetectable in mII oocytes. This implies that in mammals the Ca^{2+} signal is primarily transduced by CaMKIIγ to downregulate Emi2 activity (Chang et al., 2009; Backs

et al., 2010). We identified two isoforms of oocyte CaMKIIγ, present in equimolar amounts, raising the question of whether CaMKIIγ mediates dual regulation of Emi2 or only one of the isoforms is essential. In other cell types, CaMKII splice variants exhibit distinctive protein interactions that influence CaMKII activity directly and/or by influencing subcellular targeting (Bayer et al., 1998; Hudmon and Schulman, 2002; Gangopadhyay et al., 2008). CaMKIIγ splice variants that affect protein binding include G-2, which associates specifically with the PP2C-type phosphatase SCP3; the G-2 isoform shares a variant region with the γJ isoform present in oocytes (Gangopadhyay et al., 2003; Gangopadhyay et al., 2008). Interactions have been shown to modulate CaMKII activity through allosteric mechanisms that promote substrate phosphorylation in vivo but only poorly in vitro (e.g. Lu et al., 2003). This may explain why CaMKIIγ did not phosphorylate Emi2 in vitro, with the clear implication that one or more accessory proteins are required. One goal of future work will be to validate this and identify the adaptor molecule(s) responsible.

The machinery responsible for Ca^{2+}-induced Emi2 degradation in mouse oocytes is highly specialized. Neither Emi1, β-Catenin nor Bora – which undergo Plk- and Ca^{2+}-dependent proteasomal degradation in response to cell cycle progression – were degraded in oocytes treated with SrCl$_2$ (see Fig. S11A in the supplementary material). Emi2 degradation was not sensitive to the removal of Cdc20; Cdc20 is an APC activator required for mII exit (see Fig. S11B in the supplementary material) (Shoji et al., 2006). This is consistent with the situation in *Xenopus*, in which xEmi2 degradation requires βTrcp, a component of the E3 ubiquitin ligase, SCF (Tung et al., 2005). Using mII oocytes from gene-targeted females that lack one of the two mouse βTrcp isoforms, Trcpb1, we provide strong evidence that Trcpb1 is dispensable for Emi2 degradation (Fig. 5E). As *Trcpb1$^{-/-}$ null* female mice exhibit normal fertility (Nakayama et al., 2003), it is possible either that Trcpb1 plays no physiological role in Emi2 removal during fertilization, or that Trcpb2 and/or additional E3 ubiquitin ligases can efficiently compensate when it is absent.

Competing interests statement
The authors declare no competing financial interests.

Supplementary material
Supplementary material for this article is available at
http://dev.biologists.org/lookup/suppl/doi:10.1242/dev.052480/-/DC1

References
Amanai, M., Shoji, S., Yoshida, N., Brahmajosyula, M. and Perry, A. C. F. (2006). Injection of mammalian metaphase II oocytes with short interfering RNAs to dissect meiotic and early mitotic events. *Biol. Reprod.* **75**, 891-898.
Backs, J., Stein, P., Backs, T., Duncan, F. E., Grueter, C. E., McAnally, J., Qi, X., Schultz, R. M. and Olson, E. N. (2010). The gamma isoform of CaM kinase II controls mouse egg activation by regulating cell cycle resumption. *Proc. Natl. Acad. Sci. USA* **107**, 81-86.
Bayer, K. U., Harbers, K. and Schulman, H. (1998). αKAP is an anchoring protein for a novel CaM kinase II isoform in skeletal muscle. *EMBO J.* **17**, 5598-5605.
Bhatt, R. R. and Ferrell, J. E. (1999). The protein kinase p90 rsk as an essential mediator of cytostatic factor activity. *Science* **286**, 1362-1365.
Bouniol-Baly, C., Hamraoui, L., Guibert, J., Beaujean, N., Szöllösi, M. S. and Debey, P. (1999). Differential transcriptional activity associated with chromatin configuration in fully grown mouse germinal vesicle oocytes. *Biol. Reprod.* **60**, 580-587.
Chang, H. Y., Minahan, K., Merriman, J. A. and Jones, K. T. (2009). Calmodulin-dependent protein kinase gamma 3 (CamKIIg3) mediates the cell

cycle resumption of metaphase II eggs in mouse. *Development* **136**, 4077-4081.

Choi, T., Fukasawa, K., Zhou, R., Tessarollo, L., Borror, K., Resau, J. and Vande Woude, G. F. (1996). The Mos/mitogen-activated protein kinase (MAPK) pathway regulates the size and degradation of the first polar body in maturing mouse oocytes. *Proc. Natl. Acad. Sci. USA* **93**, 7032-7035.

Dumont, J., Umbhauer, M., Rassinier, P., Hanauer, A. and Verlhac, M. H. (2005). p90Rsk is not involved in cytostatic factor arrest in mouse oocytes. *J. Cell Biol.* **169**, 227-231.

Gangopadhyay, S. S., Barber, A. L., Gallant, C., Grabarek, Z., Smith, J. L. and Morgan, K. G. (2003). Differential functional properties of calmodulin-dependent protein kinase IIγ variants isolated from smooth muscle. *Biochem. J.* **372**, 347-357.

Gangopadhyay, S. S., Gallant, C., Sundberg, E. J., Lane, W. S. and Morgan, K. G. (2008). Regulation of Ca^{2+}/calmodulin kinase II by a small C-terminal domain phosphatase. *Biochem. J.* **412**, 507-516.

Gautier, J., Matsukawa, T., Nurse, P. and Maller, J. (1989). Dephosphorylation and activation of *Xenopus* p34cdc2 protein kinase during the cell cycle. *Nature* **339**, 626-629.

Gautier, J., Minshull, J., Lohka, M., Glotzer, M., Hunt, T. and Maller, J. L. (1990). Cyclin is a component of maturation-promoting factor from *Xenopus*. *Cell* **60**, 487-494.

Glotzer, M., Murray, A. W. and Kirschner, M. W. (1991). Cyclin is degraded by the ubiquitin pathway. *Nature* **349**, 132-138.

Gross, S. D., Schwab, M. S., Taieb, F. E., Lewellyn, A. L., Qian, Y. W. and Maller, J. L. (2000). The critical role of the MAP kinase pathway in meiosis II in *Xenopus* oocytes is mediated by p90(Rsk). *Curr. Biol.* **10**, 430-438.

Halet, G. (2004). PKC signaling at fertilization in mammalian eggs. *Biochim. Biophys. Acta* **1742**, 185-189.

Hudmon, A. and Schulman, H. (2002). Neuronal Ca^{2+}/calmodulin-dependent protein kinase II: the role of structure and autoregulation in cellular function. *Ann. Rev. Biochem.* **71**, 473-510.

Inoue, D., Ohe, M., Kanemori, Y., Nobui, T. and Sagata, N. (2007). A direct link of the Mos-MAPK pathway to Erp1/Emi2 in meiotic arrest of *Xenopus laevis* eggs. *Nature* **446**, 1100-1104.

Lee, B. J., Cansizoglu, A. E., Süel, K. E., Louis, T. H., Zhang, Z. and Chook, Y. M. (2006). Rules for nuclear localization sequence recognition by karyopherinβ2. *Cell* **126**, 543-558.

Lefebvre, C., Terret, M. E., Djiane, A., Rassinier, P., Maro, B. and Verlhac, M.-H. (2002). Meiotic spindle stability depends on MAPK-interacting and spindle-stabilizing protein (MISS), a new MAPK substrate. *J. Cell Biol.* **157**, 603-613.

Lu, C. S., Hodge, J. J., Mehren, J., Sun, X. X. and Griffith, L. C. (2003). Regulation of the Ca^{2+}/CaM-responsive pool of CaMKII by scaffold-dependent autophosphorylation. *Neuron* **40**, 1185-1197.

Marchler-Bauer, A., Anderson, J. B., Chitsaz, F., Derbyshire, M. K., DeWeese-Scott, C., Fong, J. H., Geer, L. Y., Geer, R. C., Gonzales, N. R. and Gwadz, M. (2009). CDD: specific functional annotation with the Conserved Domain Database. *Nucluer Acids Res.* **37**, 205-210.

Masui, Y. and Markert, C. L. (1971). Cytoplasmic control of nuclear behavior during meiotic maturation of frog oocytes. *J. Exp. Zool.* **177**, 129-145.

Miller, J. J., Summers, M. K., Hansen, D. V., Nachury, M. V., Lehman, N. L., Loktev, A. and Jackson, P. K. (2006). Emi1 stably binds and inhibits the anaphase-promoting complex/cyclosome as a pseudosubstrate inhibitor. *Genes Dev.* **20**, 2410-2420.

Mochida, S. and Hunt, T. (2007). Calcineurin is required to release *Xenopus* egg extracts from meiotic M phase. *Nature* **449**, 336-340.

Nakayama, K., Hatakeyama, S., Maruyama, S., Kikuchi, A., Onoé, K., Good, R. A. and Nakayama, K. I. (2003). Impaired degradation of inhibitory subunit of NF-κB (IκB) and β-catenin as a result of targeted disruption of the β-*TrCP1* gene. *Proc. Natl. Acad. Sci. USA* **100**, 8752-8757.

Nishiyama, T., Ohsumi, K. and Kishimoto, T. (2007a). Phosphorylation of Erp1 by p90rsk is required for cytostatic factor arrest in *Xenopus laevis* eggs. *Nature* **446**, 1096-1099.

Nishiyama, T., Yoshizaki, N., Kishimoto, T. and Ohsumi, K. (2007b). Transient activation of calcineurin is essential to initiate embryonic development in *Xenopus laevis*. *Nature* **449**, 341-345.

Ohe, M., Kawamura, Y., Ueno, H., Inoue, D., Kanemori, Y., Senoo, C., Isoda, M., Nakajo, N. and Sagata, N. (2010). Emi2 inhibition of the APC/C absolutely requires Emi2 binding via the C-terminal RL tail. *Mol. Biol. Cell* **21**, 905-913.

Perry, A. C. F. and Verlhac, M.-H. (2008). Second meiotic arrest and exit in frogs and mice. *EMBO Rep.* **9**, 246-251.

Peters, J. M. (2006). The anaphase promoting complex/cyclosome: a machine designed to destroy. *Nat. Rev. Mol. Cell Biol.* **7**, 644-656.

Rauh, N. R., Schmidt, A., Bormann, J., Nigg, E. A. and Mayer, T. U. (2005). Calcium triggers exit from meiosis II by targeting the APC/C inhibitor XErp1 for degradation. *Nature* **437**, 1048-1052.

Runft, L. L., Jaffe, L. A. and Mehlmann, L. M. (2002). Egg activation: where it all begins. *Dev. Biol.* **245**, 237-254.

Sagata, N., Watanabe, N., Vande Woude, G. F. and Ikawa, Y. (1989). The c-mos proto-oncogene product is a cytostatic factor responsible for meiotic arrest in vertebrate eggs. *Nature* **342**, 512-518.

Schmidt, A., Duncan, P. I., Rauh, N. R., Sauer, G., Fry, A. M., Nigg, E. A. and Mayer, T. U. (2005). *Xenopus* polo-like kinase Plx1 regulates XErp1, a novel inhibitor of APC/C activity. *Genes Dev.* **19**, 502-513.

Sharma, R. K., Desai, R., Waisman, D. M. and Wang, J. H. (1979). Purification and subunit structure of bovine brain modulator binding protein. *J. Biol. Chem.* **254**, 4276-4282.

Shoji, S., Yoshida, N., Amanai, M., Ohgishi, M., Fukui, T., Fujimoto, S., Nakano, Y., Kajikawa, E. and Perry, A. C. F. (2006). Mammalian Emi2 mediates cytostatic arrest and transduces the signal for meiotic exit via Cdc20. *EMBO J.* **25**, 834-845.

Stewart, A. A., Ingebritsen, T. S. and Cohen, P. (1983). The protein phosphatases involved in cellular regulation. 5. Purification and properties of a Ca^{2+}/calmodulin-dependent protein phosphatase (2B) from rabbit skeletal muscle. *Eur. J. Biochem.* **132**, 289-295.

Suzuki, T., Yoshida, N., Suzuki, E., Okuda, E. and Perry, A. C. F. (2010). Full-term mouse development by abolishing Zn^{2+}-dependent metaphase II arrest without Ca^{2+} release. *Development* **137**, 2659-2669.

Tang, W., Wu, J. Q., Chen, C., Yang, C. S., Guo, J. Y., Freel, C. D. and Kornbluth, S. A. (2010). Emi2-mediated inhibition of E2-substrate ubiquitin transfer by the APC/C through a D-Box-independent mechanism. *Mol. Biol. Cell.* Epub ahead of print.

Terret, M. E., Lefebvre, C., Djiane, A., Rassinier, P., Moreau, J., Maro, B. and Verlhac, M.-H. (2003). DOC1R: a MAP kinase substrate that control microtubule organization of metaphase II mouse oocytes. *Development* **130**, 5169-5177.

Tung, J. J., Hansen, D. V., Ban, K. H., Loktev, A. V., Summers, M. K., Adler, J. R. and Jackson, P. K. (2005). A role for the anaphase-promoting complex inhibitor Emi2/XErp1, a homolog of early mitotic inhibitor 1, in cytostatic factor arrest of Xenopus eggs. *Proc. Natl. Acad. Sci. USA* **102**, 4318-4323.

Verlhac, M. H., Kubiak, J. Z., Weber, M., Geraud, G., Colledge, W. H., Evans, M. J. and Maro, B. (1996). Mos is required for MAP kinase activation and is involved in microtubule organization during meiotic maturation in the mouse. *Development* **122**, 815-822.

Webb, M., Howlett, S. K. and Maro, B. (1986). Parthenogenesis and cytoskeletal organization in ageing mouse eggs. *J. Embryol. Exp. Morphol.* **95**, 131-145.

Wu, J. Q. and Kornbluth, S. (2008). Across the meiotic divide-CSF activity in the post-Emi2/XErp1 era. *J. Cell Sci.* **121**, 3509-3514.

Wu, J. Q., Hansen, D. V., Guo, Y., Wang, M. Z., Tang, W., Freel, C. D., Tung, J. J., Jackson, P. K. and Kornbluth, S. (2007a). Control of Emi2 activity and stability through Mos-mediated recruitment of PP2A. *Proc. Natl. Acad. Sci. USA* **104**, 16564-16569.

Wu, Q., Guo, Y., Yamada, A., Perry, J. A., Wang, M. Z., Araki, M., Freel, C. D., Tung, J. J., Tang, W., Margolis, S. S. et al. (2007b). A role for Cdc2- and PP2A-mediated regulation of Emi2 in the maintenance of CSF arrest. *Curr. Biol.* **17**, 213-224.

Yoshida, N., Brahmajosyula, M., Shoji, S., Amanai, M. and Perry, A. C. F. (2007). Epigenetic discrimination by mouse metaphase II oocytes mediates asymmetric chromatin remodeling independently of meiotic exit. *Dev. Biol.* **301**, 464-477.